IEEE Photonics Journal
An IEEE Photonics Society Publication

Spectrum Intensity Ratio Detection for Frequency Domain Weak Measurement System

Volume 12, Number 4, August 2020

Yuxuan Yang
Yang Xu
Tian Guan
Lixuan Shi
Jinyu Li
Dongmei Li
Yonghong He
Xiangnan Wang
Zhangyan Li
Yanhong Ji

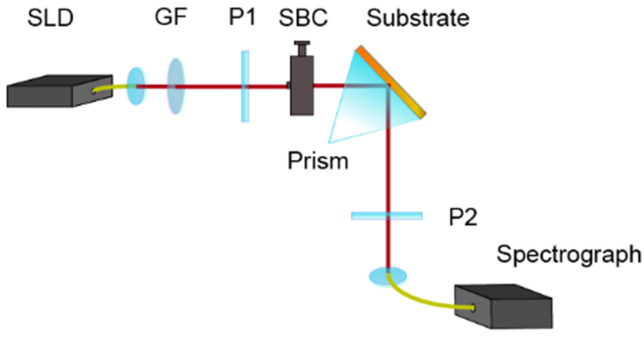

DOI: 10.1109/JPHOT.2019.2942718

Spectrum Intensity Ratio Detection for Frequency Domain Weak Measurement System

Yuxuan Yang,[1,2] Yang Xu,[2] Tian Guan,[1,2] Lixuan Shi,[2,3] Jinyu Li,[4] Dongmei Li,[5] Yonghong He,[2,3] Xiangnan Wang,[1,2] Zhangyan Li,[2,3] and Yanhong Ji[6]

[1]Department of Biomedical Engineering, School of Medicine, Tsinghua University, Beijing 100084, China
[2]Shenzhen Key Laboratory for Minimal Invasive Medical Technologies, Institute of Optical Imaging and Sensing, Graduate School at Shenzhen, Tsinghua University, Shenzhen 518055, China
[3]Department of Physics, Tsinghua University, Beijing 100084, China
[4]State Key Laboratory of Alternate Electrical Power System With Renewable Energy Sources, North China Electric Power University, Beijing 102206, China
[5]Center for Optics & Optoelectronics Research, Collaborative Innovation Center for Information Technology in Biological and Medical Physics, College of Science, Zhejiang University of Technology, Hangzhou 310023, China
[6]School of Physics and Telecommunication Engineering, South China Normal University, Guangzhou 510006, China

DOI:10.1109/JPHOT.2019.2942718

Manuscript received April 16, 2019; revised August 27, 2019; accepted September 10, 2019. Date of publication October 10, 2020; date of current version June 29, 2020. This research was made possible with the financial support from National Science Foundation of China (NSFC) (61875102, 81871395, 61675113), Science and Technology Research Program of Shenzhen City (JCYJ20170816161836562, JCYJ20170817111912585, JCYJ20160427183803458, JCYJ20170412171856582, JCY20180508152528735). (Yuxuan Yang and Yang Xu contributed equally to this work.) Corresponding authors: Yonghong He; Tian Guan (e-mail: Heheyh@sz.tsinghua.edu.cn; guantian@sz.tsinghua.edu.cn).

Abstract: The traditional method of frequency domain weak measurement has a lot of noise. In this paper, we analyze the 2000 curves obtained by experiments and get the conclusion that the signal-to-noise ratio will increase with the increase of signal strength. We simulated the 252 curves produced by the phase change and used this to fit the relationship between the original calculation method and our spectral height ratio (HR) method. Through previous experimental data verification, our method can greatly reduce the system noise of the dual-mode working area in the frequency domain weak measurement. At present, universal frequency domain weak measurement and measurement system have received increasing attention. In this paper, we introduce a frequency domain weak measurement with spectrum height ratio (HR) that can greatly reduce the system noise in the frequency domain weak measurement bimodal work area. Moreover, we completed comparative experiments on a total internal reflection weak measurement system. The experimental results show that the system resolution obtained by using the HR method is 6.33×10^{-7} RIU, which is an order of magnitude higher than that of the conventional center wavelength offset algorithm which is commonly used in weak frequency measurement.

Index Terms: Noise analysis, optical biosensor, weak measurement, resolution improvement, spectrum height ratio.

1. Introduction

The weak measurement was proposed by AAV in 1988 and was first confirmed by Ritchie *et al.* in 1991 [1], [2]. In weak measurements we refer to this process of amplifying the parameters we actually need as Weak Value Amplification (WVA). Weak measurement techniques are important in the interpretation of quantum physics phenomena [3], [4] and in precision metrology [5], [6]. At present, weak measurement techniques have been widely used in various measurements, such as: Gushi-Hanchen shift [7], polarization rotation [8], temperature [9], and phase shift [10], beam deflection [11], sub-pulse width time delay [12].

Subsequently, Brunner *et al.* proposed that weak measurement method using the imaginary weak value amplification can result in 3 orders of magnitude higher than the traditional interference method [13], namely the frequency domain weak value amplification technique. Frequency-domain weak measurement amplification technology is currently used in the field of biosensors, such as the combination of weak measurement technology and Mach–Zehnder interferometer to measure mouse blood glucose concentration [14], and combining weak measurement technology with total internal reflection (TIR) sensors to realize real-time monitoring of biological Macromolecular interactions [15], weak measurement techniques applied to the detection of chiral molecules [16], optical rotation of DNA molecules [17], optimization of weak measurement techniques [18], [19], multifunctional weak measurement system [20]. Combining weak measurement technology with total internal reflection (TIR) sensors has more application prospects due to its high stability, good robustness, high detection sensitivity and low detection cost. It has advantages over some detection techniques that require surface modification, such as surface plasmon resonance technology [21], [22], in terms of complexity and cost of detection. Although the sensitivity of such sensors is greatly improved, the bimodal center wavelength offset algorithm that we now use to process data is greatly affected by the overall noise of the weak measurement system, which in turn results in a lower resolution of the weak measurement sensor.

And we took the two sets of curves in the actual experiment and found that there is a positive correlation between signal to noise ratio (SNR) and signal strength. The traditional center wavelength shift (CWS) calculation method that calculates all the signals will also calculate the area with lower SNR, which seriously affects the center wavelength stability. So a new high-resolution data processing method which can prevent stability from being affected by lower SNR areas needs to be put forward.

In this paper, we introduced a new ratio algorithm that can be applied to frequency domain weak measurements. This method only used the area with higher SNR to calculate the relevant parameters, which avoided the disadvantage that the traditional method will be greatly affected by the poor SNR area. We derived the simulation of the relationship between CWS and HR, and obtained the relationship between the two methods. Furthermore, we completed the experimental verification under a TIR weak measurement sensor system. We added different concentrations of sodium chloride solution to the TIR weak measurement system. We used the traditional CWS algorithm and the new proposed frequency-domain weak-measurement HR algorithm to process obtained data. The experimental results showed that using HR to process data can significantly improve the data stability, and the system resolution can reach 6.33×10^{-7}. Compared with the resolution 6.68×10^{-6} obtained by the conventional CWS algorithm, the resolution of the weak measurement system was increased by one order of magnitude.

2. Materials and Methods

The weak value amplification (WVA) comes from the weak measurement. We build up the measuring process by the measuring system and the measuring device, the measuring device is weak coupled with the measuring system. We measure the system state in order to indirectly observe the device state. If the system state is pre-selected and post-selected in a proper way, we can obtain an amplification in weak value. Fig. 1 shows the experimental devices. We choose polarization state as the selected system state, and use polarizers for pre- and post-selection. After the pre-selection

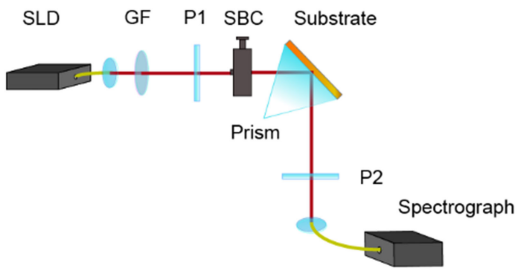

Fig. 1. Experimental setup. 830 nm Gaussian filter with a bandwidth of 20 nm; Polarizers (ThorlabsInc., LPVIS050-MP, extinction ratio of 100000:1) P1 for pre-selection and P2 for post-selections, respectively; K9 prism and substrate with refractive index matching liquid; SBC, Soleil-Babinet compensator; Light source, superluminent laser diode (SLD, SLD830S-A20,830 nm, 5 mW, Thorlabs Inc.) and spectrometer omitted; Spectrograph (OceanOptiocs, HR2000).

polarizer, the beam passes through a Soleil Babinet compensator (SBC), and the polarization operator is coupled with the photon longitudinal momentum. It is worth noticed that weak value amplification does not provide more information of the measurement itself. However, WVA, by costing of lower detection probability, gains a higher sensitivity advantage.

In this paper, the experimental method is validated by the reflective phase sensitive weak measurement method. However, HR is applicable to any form of frequency domain weak measurement system and is not limited to reflective systems. The schematic diagram of weak measurement system is shown in Fig. 1. In this paper, the experimental method is validated by the reflective phase sensitive weak measurement method. However, HR is applicable to any form of frequency domain weak measurement system and is not limited to reflective systems. The schematic diagram of weak measurement system is shown in Fig. 1.

The light emitted by the superluminescent diode (SLD,830 nm, 5 mW, Thorlabs Inc.) passes through the collimating lens, the Gaussian filter (center wavelength 830 nm, FWHM 10 nm), the pre-selected polarizer (Thorlabs LPVIS050-MP, extinction ratio is 100000:1), and the K9 prism with a refractive index of 1.51 (the light is totally reflected at the incident angle of 45° on the substrate of the K9 prism, greater than the critical angle which calculated as 59.4°), Soleil Babinet compensator (SBC, Thorlabs Inc., SBC-IR), post-selected polarizer, the collimator lens is finally received by the spectrometer (OceanOptiocs, HR4000).

The phase difference increases depending on the refractive index, but TIR does not cause the light intensity decrease.

$$\Delta = 2\tan^{-1}\frac{\sqrt{n^2\sin^2\theta - 1}}{n\sin\theta\tan\theta}, \tag{1}$$

Here θ represents the incident angle of light, and n = n1/n2. n1, and n2 are refractive indices of the prism and the analytes, respectively. After the prism, the beam passes through an SBC modulator. By adjusting the SBC, we can modulate the phase difference between *p* and *s* polarized light. The phase difference leads to spectral shift in the imaginary part of the weak value.

We predict and simulate the spectra obtained after the post-selection state. In the same way, we write the initial state of the system as $|\Psi_i\rangle = |\psi_i\rangle|\psi_p\rangle$, The polarization state $\langle\psi_i| = \alpha|H\rangle + \beta|V\rangle$, $|\psi_p\rangle$ is the state of the momentum of the conjugate of the gauge pointer. The initial spectrum is a Gaussian spectrum. The observable operator A acts on two eigenstates and obtains $A|H\rangle = |H\rangle$, $A|V\rangle = -1|V\rangle$. When the photon passes through the SBC, due to the effect of the propagation direction, the momentum of the photon has changed slightly. According to Aharonov's theory [14], Hamiltonian can be written as H = g(t)PA, where g is a short-term interaction strength and P is a momentum operator. After the interaction, the state of the system changes.

$$\left|\psi_p\right\rangle \sim I_0 \cdot e^{-\frac{(p-p_0)^2}{2\delta_p{}^2}}, \tag{2}$$

$$U\left|\psi_i\right\rangle\left|\psi_p\right\rangle = \alpha e^{-igP}\left|\psi_p\right\rangle|H\rangle + \beta e^{igP}\left|\psi_p\right\rangle|V\rangle, \tag{3}$$

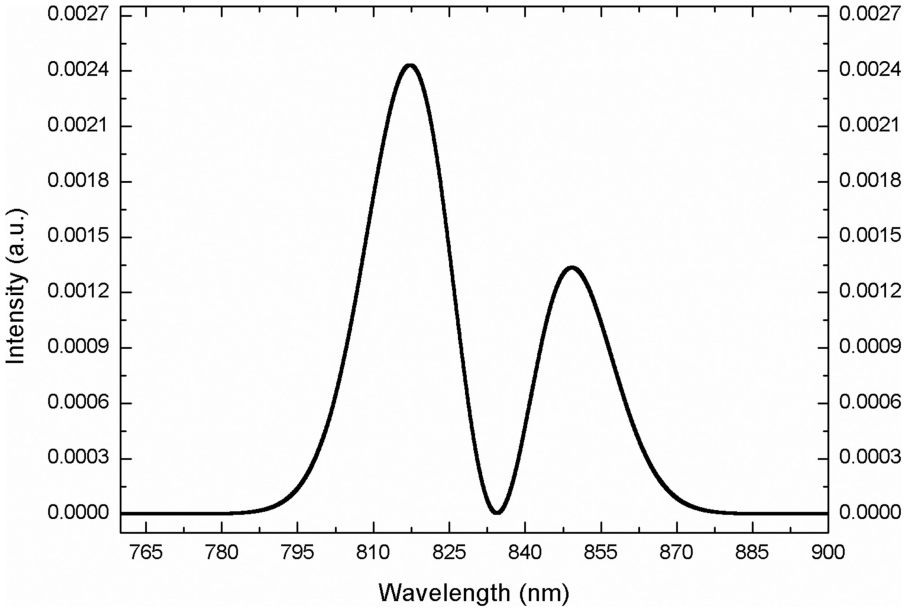

Fig. 2. Experimental spectral shape. The weak measurement in the frequency domain is most sensitive to the refractive index transformation in this double-peak range, so this region is often chosen as the weak-frequency-domain measurement work region.

We choose the post-selection state: $|\psi_f\rangle = u|H\rangle + v|V\rangle$. After applying the post-selection state, the state of the system can be written as:

$$\left|\psi_f\right\rangle = \left\langle\psi_f\right| \left|\psi_i\right\rangle \left|\psi_p\right\rangle = \left\langle\psi_f\right| U \left|\psi_i\right\rangle \left|\psi_p\right\rangle = u^*\alpha e^{-igP} \left|\psi_p\right\rangle + v^*\beta e^{igP} \left|\psi_p\right\rangle, \tag{4}$$

Then the final measurement results can be written as:

$$\left\langle\psi_f\right| \left|\psi_f\right\rangle = \left|u^*\alpha e^{-igP} + v^*\beta e^{igP}\right|^2 e^{\left[-\frac{(p-p_0)^2}{2\delta p^2}\right]}, \tag{5}$$

According to the definition of weak value,

$$A_\omega \equiv \frac{\left\langle\psi_f\right| A \left|\psi_i\right\rangle}{\left\langle\psi_f \mid \psi_i\right\rangle} = \frac{u^*\alpha - v^*\beta}{u^*\alpha + v^*\beta}, \tag{6}$$

We let $u^*\alpha = a$, $v^*\beta = b$, according to Eq. 4, we can get:

$$\left|u^*\alpha e^{-igP} + v^*\beta e^{igP}\right|^2 = \left|(a+b)\cos(pg) + i(b-a)\sin(pg)\right|^2 = |a+b|^2 \cdot \left|[\cos(pg) - iA_\omega \sin(pg)]\right|^2, \tag{7}$$

Here we use the imaginary part of A_ω, so we can express Eq. 4 as:

$$\left\langle\psi_f\right| \left|\psi_f\right\rangle = |a+b|^2 \cdot \left|\cos(pg) + ImA_\omega \sin(pg)\right|^2 e^{\left[-\frac{(p-p_0)^2}{2\delta p^2}\right]}, \tag{8}$$

We can see that when the weak value is very small, that is, the orthogonality between the post-selection state and the pre-selection state is relatively poor, the Eq. 8 mesophase is close to a constant, and the resulting signal spectrum is still a Gaussian type which only has a small offset at the center wavelength. When the rear selection state gradually approaches the vertical, the weak value increases, and the resulting spectral image may have two peaks. The common spectral shape during the experiment is as follows:

In our actual experimental signals, the areas with large noise are not evenly distributed, that is, the signal-to-noise ratio (SNR) is positively correlated with the signal strength. We performed analyses of two aspects on two sets of double-peak curves with different sizes. And get Fig. 3(a) which is

$SNR_{L1-1} = 436.08$， $SNR_{L1-2} = 1064.81, SNR_{L1-3} = 2478.35, SNR_{L1-4} = 4437.53$

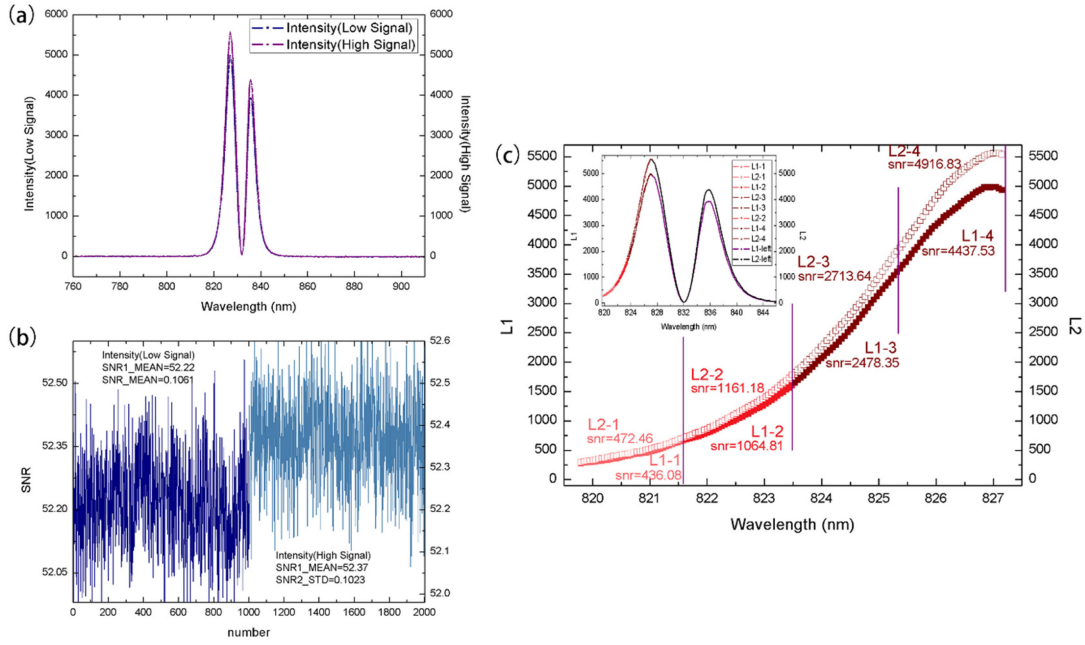

$SNR_{L2-1} = 472.46$， $SNR_{L2-2} = 1161.18, SNR_{L2-3} = 2713.64, SNR_{L2-4} = 4916.83$

Fig. 3. (a) Two sets of bimodal curves we analyzed represents different signal strength. (b) The average SNR of the L2 group and the L1 group. (c) The average SNR of the typical area segmentation calculation.

the two sets of bimodal curves we analyzed. There are 1000 double-peak curves in each group. The signal intensity of 1000 double-peak curves in each group is basically the same. The blue line group representing the weaker signal is L1, and the purple line group representing the stronger signal is L2. We first find the SNR of the entire curve of 2000 curves of L1 and L2, respectively, and obtain the magnitudes of the two sets of SNR as shown in Fig. 1(b). We calculated that the average SNR of the L2 group representing the stronger signal is 52.37, which is better than the average SNR of the L1 group representing the weaker signal of 52.22. We then select the typical regions of the two curves, as shown in Fig. 1(c). The SNR is segmented and calculated. L1 and L2 are respectively cut into 140 points in the monotonously growing region of the first half, and each 35 points are divided into one segment and a total of four segments, which can be obtained as shown in Fig. 1(c). The difference between the two sets of SNR amplitudes can be obtained, and the SNR of each segment can be obtained.

In the same curve L1 or L2, the SNR of the signal with stronger signal strength is also significantly better than the signal with weaker signal strength. Therefore, the reason why the actual experimental data fluctuates greatly is because the SNR of the low-intensity signal is too small to lower the overall level. We decided to try to select some areas with better SNR to express the experimental results, instead of the traditional CWS algorithm which is calculated together for all regions.

We observed that the two peaks of the weakly measured emission spectrum change as shown in the figure. When we use the system for weak measurement, the most sensitive measurement interval we use is the bimodal change region, and the two purple single peaks in Fig. 4(a) are removed to obtain the common measurement as shown in Fig. 4(b).

After our calculation, in the bimodal measurement area shown, the traditional CWS changes monotonously with the phase change, but we observe that the double peak phenomenon of “one increase and one drop monotonously” is also very obvious. That is to say, the height ratio of the peak of the A peak in the front and the peak of the B peak in the back in spectrum figure is also monotonously changed with the phase change. The method of HR calculation is equivalent

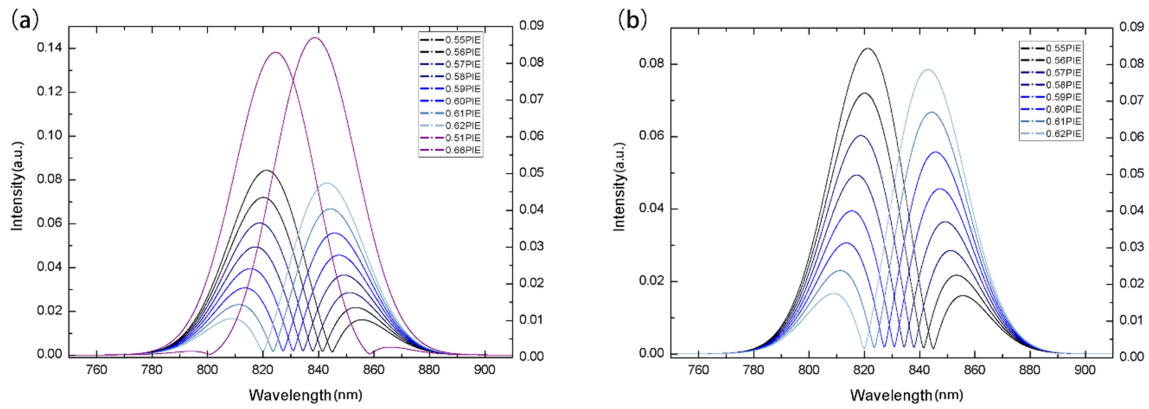

Fig. 4. (a) Schematic diagram of measurement signal as a function of phase (including infrequent areas). (b) Schematic diagram of measurement signal as a function of phase (only common areas).

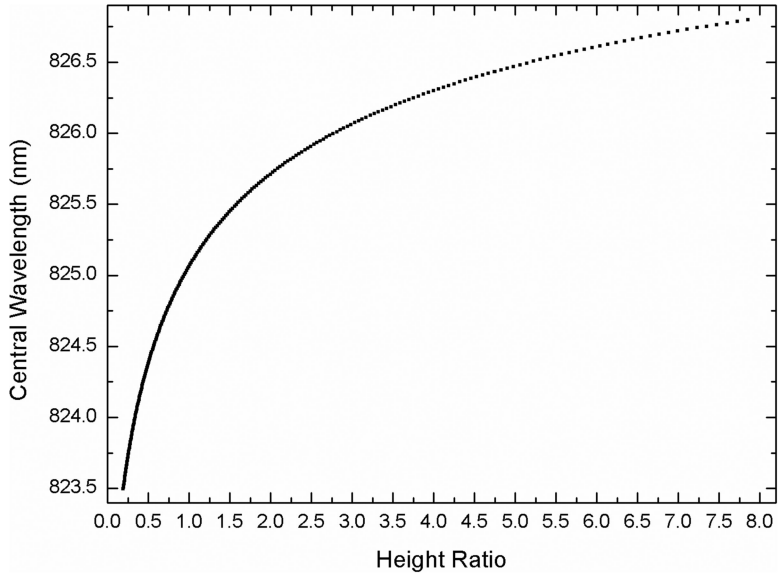

Fig. 5. Relationship between center wavelength (CWS) and peak ratio (HR).

to selecting the area with high SNR for calculation, which solves the problem that the SNR of traditional CWS algorithm is too large and can improve the resolution of the measurement system.

So we proposed a new frequency domain weak measurement ratio algorithm. We take the peaks of the peak of the A peak in the front and the peak of the B peak in the back in spectrum figure respectively, Hmax1 and Hmax2. Then according to the Eq. 9:

$$\mathrm{HR} = \frac{\mathrm{Hmax1}}{\mathrm{Hmax2}}, \tag{9}$$

We use MATLAB to calculate the changes of CWS and HR for the total of 252 bimodal curves when the phase is from 0.55π to 0.63π. That is to simulate the change of two calculated indicators produced when the state of the substance to be tested changes, so as to analyze the relationship between the two calculated indexes of CWS and HR, and obtain the corresponding changes of CWS and HR when the phase changes in Fig. 5. We then want to analyze the relationship between CWS and HR, so HR is plotted on the abscissa and CWS is plotted on the ordinate in Fig. 5.

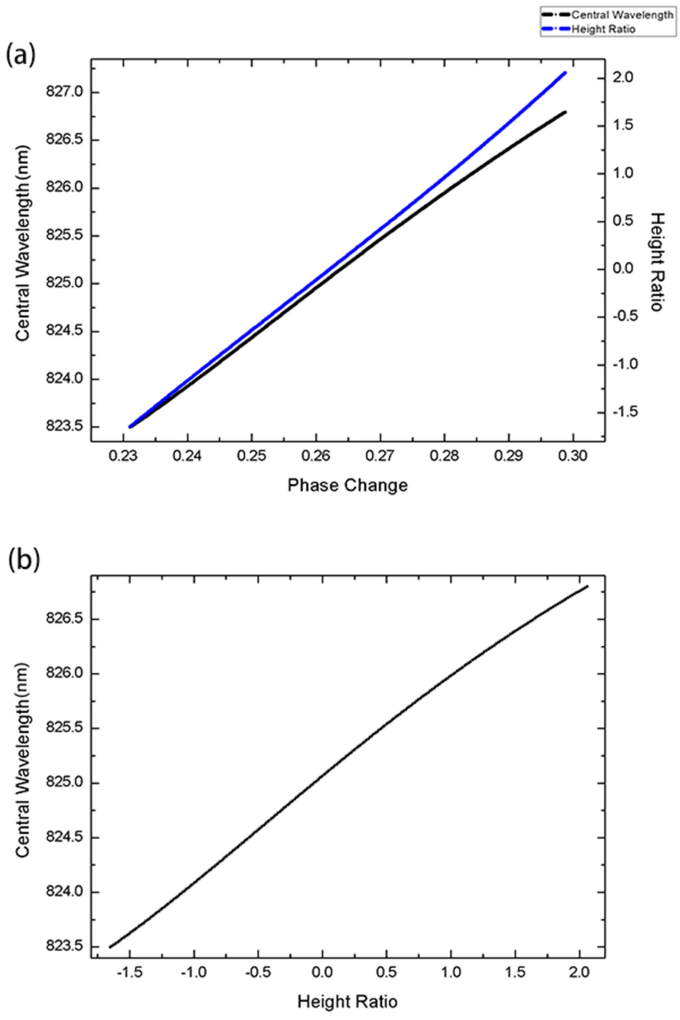

Fig. 6. (a) Relationship between CWS, natural logarithm of HR with phase change. (b) Relationship between CWS and natural logarithm of HR.

In Fig. 5 we can see that the relationship between CWS and HR is a log-like relationship, and HR and phase change are a log-like relationship in Fig. 5. For this reason, we try to take the natural logarithm of the HR-phase curve and get the two lines as shown in Fig. 6. In Fig. 6(a) we can see that the natural logarithm of HR approximates a straight line. We also draw the Fig. 6(b) with the natural logarithm of HR as the abscissa and CWS as the ordinate, and we get an approximate straight line.

We use the polyfit and polyval functions in MATLAB to determine the order of this approximate line. When the fitting order is 1, we can reduce the error to below 0.1 and reach the fitting condition. Furthermore, the polyfit function is used to fit the curve in 1st order, and the relationship between CWS and natural logarithm of HR is obtained, and the relationship between HR and CWS can be obtained. Furthermore, the relationship between HR and phase change can be obtained according to the relationship between CWS and phase change in the foregoing:

$$\mathrm{CWS} = 54.021475 \times \ln(HR) - 6.040856 \tag{10}$$

That is,

$$\mathrm{HR} = e^{\frac{\mathrm{CWS}+6.040856}{54.021475}} \tag{11}$$

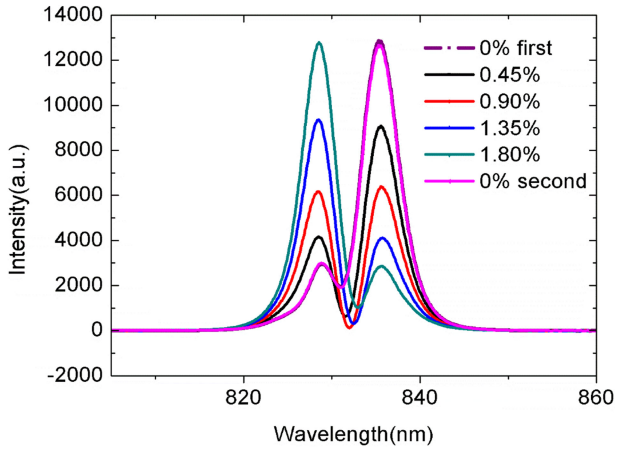

Fig. 7. Five-concentration sodium chloride solution bimodal image.

For this we have done a verification test.

3. Results

We first introduced deionized water into the flow cell on the surface of the prism, and then adjusted the total internal reflection sensor to a highly sensitive bimodal working region based on weak measurement techniques. After the system is stable, the data is recorded by the OceanOptiocs spectrometer using its own program. After that, four concentrations of sodium chloride solution were introduced successively at concentrations of 0.45%, 0.90%, 1.35%, and 1.80%. The concentration dependence of the refractive index of the sodium chloride solution is 1.47×10^{-3} C [23], where C is the mass percentage. Therefore 0.45%, 0.90%, 1.35%, and 1.8% sodium chloride solutions caused refractive index changes of 0.662×10^{-3} RIU, 1.323×10^{-3} RIU, 1.984×10^{-3} RIU, and 2.646×10^{-3} RIU, respectively. As shown in Fig. 7, bimodal image data of four concentrations of sodium chloride solution at concentrations of 0.45%, 0.90%, 1.35%, and 1.80% were collected and recorded, respectively. The solution was then passed into deionized water, which means the solution was passed in the order of 0%, 0.45%, 0.90%, 1.35%, 1.80% and 0% to verify the repeatability of the system. We use the bimodal center wavelength shifting algorithm of frequency domain weak measurement and our frequency domain HR to process the data.

It can be seen from the figure that when the two concentrations are 0%, the bimodal curves are coincident, and the solutions with different concentrations have the same curve shape in our system, which proves that our measurement platform is robust and repeatable.

By analyzing the shape of the corresponding curves for different concentrations of the solution, numerical values that can uniquely correspond to the shape of the curves are calculated, and the concentration of the solution is quantitatively measured. In the previous work, the method of analyzing the shape of the curves were to calculate the center wavelength of each curve, and then to associate the center wavelength of the measured value with the concentration of the solution. However, the method of calculating the center wavelength is greatly affected by the overall noise of the system, which in turn results in a low resolution of the weak measurement sensor. Because the two-peak region is the most sensitive measurement range that we usually use for measurement, and the bimodal height change is monotonous with the concentration change, and the two peaks change in the opposite direction, that is, the left peak increases with increasing concentration and the right peak decreases with increasing concentration, we propose a new high-resolution data processing method: each curve is uniquely scaled by the ratio of heights between the two peaks.

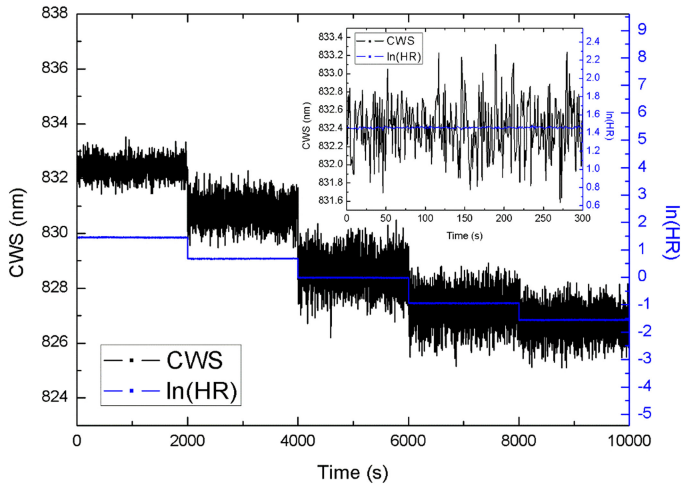

Fig. 8. Comparison of resolutions of CWS and HR algorithms: Solution concentration curve obtained using the center wavelength shift algorithm and height ratio.

3.1 Center Wavelength Shift Algorithm

We use the CWS algorithm for weak measurement in the frequency domain and the HR proposed by us to process the data. As shown in Fig. 8, a 1.8% sodium chloride solution caused a wavelength shift of 4.35 nm compared to deionized water under the CWS algorithm. The sensitivity characterized by $\delta\lambda/\delta n$ is 1662 nm/RIU.

After each solution is passed, we wait for the system to stabilize and then calculate the standard deviation of the system by averaging 100 data points. The inset of Fig. 8 shows the change in the center wavelength corresponding to a mass fraction of 1.8% sodium chloride solution within 300 s; the standard deviation σ_s is calculated to be 0.00370 nm. Therefore, as shown in Fig. 9(a), we calculate the system refractive index resolution by the formula $\sigma = 3\sigma_s/(\delta\lambda/\delta n)$ to be 6.68 $\times$ 10^{-6} RIU.

3.2 Spectrum Intensity Ratio Algorithm

Similarly, as shown in Fig. 8, we use the frequency domain HR proposed to analyze the same value. We set the unit of ratio change with refractive index as weak measurement ratio change (WMRC). As shown in Fig. 8(b), under the frequency domain HR, a 1.8% sodium chloride solution caused a change in the 2.85 WMRC compared to the deionized water. The sensitivity characterized by $\delta\lambda/\delta n$ is 1089 WMRC/RIU.

After each solution is passed, we wait for the system to stabilize and then calculate the standard deviation of the system by averaging 100 data points. The inset of Fig. 8 shows the change in the weak measurement ratio corresponding to a mass fraction of 1.8% sodium chloride solution within 300 s; the standard deviation σ_s is calculated to be 0.00023 WMRC. Therefore, as shown in Fig. 9(b), we calculate the system refractive index resolution by the formula $\sigma = 3\sigma_s/(\delta\lambda/\delta n)$ to be 6.33 $\times$ 10^{-7} RIU.

4. Discussion

We have analyzed the experimental results from another aspect. By calculating HR first, we calculate HR_CWS by formula 10. Comparing this indirect calculation with the direct calculation of CWS, as shown in Fig. 10, the stability of HR_CWS is also significantly better than the direct calculation of CWS. Therefore, it is further explained that the stability of the CWS algorithm is mainly affected by regions with low light intensity and poor SNR.

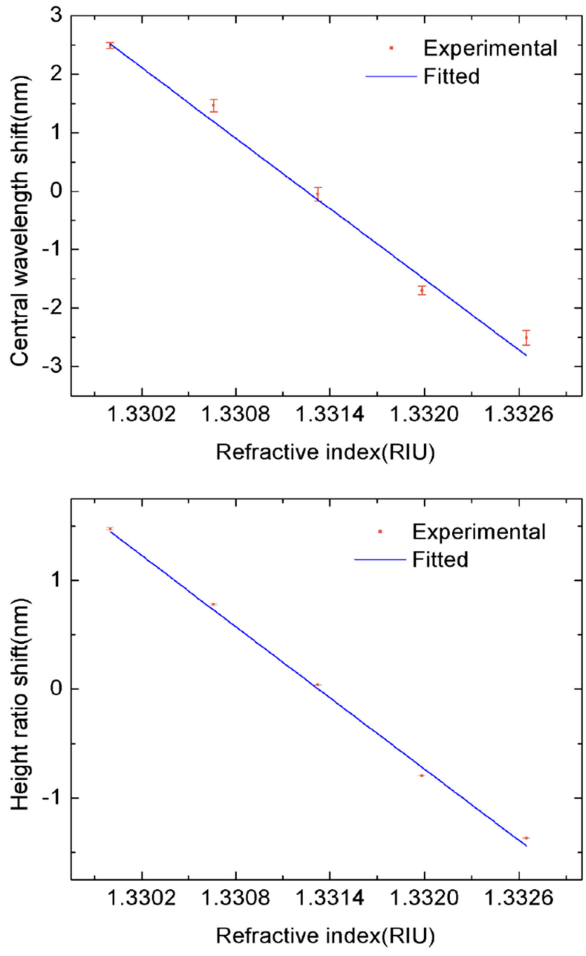

Fig. 9. Comparison of fluctuations between two algorithms for characterizing solution concentration: (a) Experimental results of dilute solution treatment by central wavelength offset algorithm; (b) Experimental results of dilute solution treatment by HR. HR has small fluctuations with respect to the central wavelength offset algorithm.

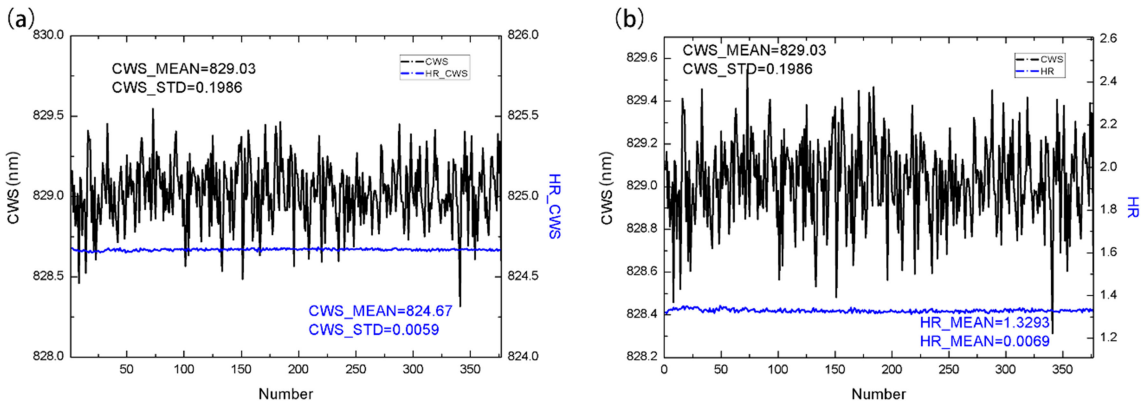

Fig. 10. (a) Comparison of volatility between direct calculation of CWS and indirect calculation of HR_CWS by HR (b) Comparison of volatility between CWS algorithm and HR algorithm.

The current optical frequency domain weak measurement system has a broad prospect in biosensors because its measurement accuracy can be three orders of magnitude higher than conventional interference detection. However, in order to get greater weak values, optical weak measurement sensor systems may loss light intensity to a certain extent. The reason above leads to the system being affected by noise caused by external factors such as light source and spectrometer, So there is a need for a method to increase the resolution of weak measurement systems. In this paper, we proposed a new frequency domain weak measurement with spectrum intensity ratio method. Compared with the traditional CWS algorithm, the HR method proposed greatly reduces the influence of external noise on the resolution of the system, which increases the resolution of the weak measurement system by an order of magnitude. However, this HR method also has some shortcomings. This HR method is effective only when the weak measurement system has a double-peak region, so the measurement range is lower than the conventional algorithm.

At present, the improved scheme of surface plasmon resonance sensor based on weak value amplification shows great advantages in resolution, which can reach 2.9×10^{-7} RIU [24]. It can be seen that the resolution of the weak measurement sensor obtained in our work is similar to the resolution of this surface plasmon resonance sensor based on weak amplification.

5. Conclusions

In summary, we proposed a new algorithm for frequency-domain weak measurement dual-peak working region—frequency-domain weak measurement with spectrum intensity ratio (HR). And we carried out experimental verification in the total internal reflection of weak total measurement system. The experimental results show that compared with the common center wavelength shift algorithm in the field of weak frequency measurement, the HR can greatly reduce the impact of the overall system noise, and thus the system resolution has been significantly improved. In this experiment, we obtained the weak measurement system resolution of 6.33×10^{-7} RIU by the frequency domain HR, which is higher than the 6.68×10^{-6} RIU obtained by the common center wavelength shift algorithm by an order of magnitude.

Acknowledgment

The authors declare that they have no conflict of interest.

References

[1] Y. Aharonov, D. Z. Albert, and L. Vaidman, "How the result of a measurement of a component of the spin of a spin-1/2 particle can turn out to be 100," *Phys. Rev. Lett.*, vol. 60, no. 14, pp. 1351–1354, Apr. 1988, doi: 10.1103/PhysRevLett.60.1351.

[2] N. W. M. Ritchie, J. G. Story, and R. G. Hulet, "Realization of a measurement of a 'weak value'," *Phys. Rev. Lett.*, vol. 66, no. 9, pp. 1107–1110, Mar. 1991, doi: 10.1103/PhysRevLett.66.1107.

[3] O. Hosten and P. Kwiat, "Observation of the spin Hall effect of light via weak measurements," *Science*, vol. 319, no. 5864, pp. 787–790, Feb. 2008, doi: 10.1126/science.1152697.

[4] T. Denkmayr *et al.*, "Observation of a quantum Cheshire Cat in a matter-wave interferometer experiment," *Nature Commun.*, vol. 5, Jul. 2014, Art. no. 4492, doi: 10.1038/ncomms5492.

[5] J. Dressel, M. Malik, F. M. Miatto, A. N. Jordan, and R. W. Boyd, "Colloquium: Understanding quantum weak values: Basics and applications," *Rev. Modern Phys.*, vol. 86, no. 1, pp. 307–316, Mar. 2014, doi: 10.1103/RevModPhys.86.307.

[6] S. Pang and T. A. Brun, "Improving the precision of weak measurements by postselection measurement," *Phys. Rev. Lett.*, vol. 115, no. 12, Sep. 2015, Art. no. 120401, doi: 10.1103/PhysRevLett.115.120401.

[7] G. Jayaswal, G. Mistura, and M. Merano, "Weak measurement of the Goos–Hänchen shift," *Opt. Lett.*, vol. 38, no. 8, pp. 1232–1234, Apr. 2013, doi: 10.1364/OL.38.001232.

[8] B. de Lima Bernardo, S. Azevedo, and A. Rosas, "Ultrasmall polarization rotation measurements via weak value amplification," *Phys. Lett. A*, vol. 378, no. 30/31, pp. 2029–2033, Jun. 2014, doi: 10.1016/j.physleta.2014.05.009.

[9] L. J. Salazar-Serrano *et al.*, "Enhancement of the sensitivity of a temperature sensor based on fiber Bragg gratings via weak value amplification," *Opt. Lett.*, vol. 40, no. 17, pp. 3962–3965, Sep. 2015, doi: 10.1364/OL.40.003962.

[10] X. Y. Xu, Y. Kedem, K. Sun, L. Vaidman, C. F. Li, and G. C. Guo, "Phase estimation with weak measurement using a white light source," *Phys. Rev. Lett.*, vol. 111, no. 3, Jul. 2013, Art. no. 033604, doi: 10.1103/PhysRevLett.111.033604.

[11] P. B. Dixon, D. J. Starling, A. N. Jordan, and J. C. Howell, "Ultrasensitive beam deflection measurement via interferometric weak value amplification," *Phys. Rev. Lett.*, vol. 102, no. 17, May 2009, Art. no. 173601, doi: 10.1103/PhysRevLett.102.173601.
[12] L. J. Salazar-Serrano, D. Janner, N. Brunner, V. Pruneri, and J. P. Torres, "Measurement of sub-pulse-width temporal delays via spectral interference induced by weak value amplification," *Phys. Rev. A*, vol. 89, no. 1, Jan. 2014, Art. no. 012126, doi: 10.1103/PhysRevA.89.012126.
[13] N. Brunner and C. Simon, "Measuring small longitudinal phase shifts: Weak measurements or standard interferometry?" *Phys. Rev. Lett.*, vol. 105, no. 1, Jul. 2010, Art. no. 010405, doi: 10.1103/PhysRevLett.105.010405.
[14] D. Li, Z. Shen, Y. He, Y. Zhang, Z. Chen, and H. Ma, "Application of quantum weak measurement for glucose concentration detection," *Appl. Opt.*, vol. 55, no. 7, pp. 1697–1702, Mar. 2016, doi: 10.1364/AO.55.001697.
[15] T. Guan *et al.*, "Determination of tumor marker carcinoembryonic antigen with biosensor based on optical quantum weak measurements," *Sensors*, vol. 18, no. 5, May 2018, Art. no. 1550, doi: 10.3390/s18051550.
[16] D. Li *et al.*, "A chiral sensor based on weak measurement for the determination of proline enantiomers in diverse measuring circumstances," *Biosens. Bioelectron.*, vol. 110, pp. 103–109, Jul. 2018, doi: 10.1016/j.bios.2018.03.033.
[17] T. Guan *et al.*, "Label-free and non-destruction determination of single- and double-strand DNA based on quantum weak measurement," *Sci. Rep.*, vol. 9, pp. 1891–1899, Feb. 2019, doi: 10.1038/s41598-018-38454-x.
[18] Y. Xu *et al.*, "Optimization of a quantum weak measurement system with digital filtering technology," *Appl. Opt.*, vol. 57, no. 27, pp. 7956–7966, Sep. 2018, doi: 10.1364/AO.57.007956.
[19] Y. Xu *et al.*, "Optimization of a quantum weak measurement system with its working areas," *Opt. Express*, vol. 26, no. 16, pp. 21119–21131, Aug. 2018, doi: 10.1364/OE.26.021119.
[20] Y. Xu *et al.*, "Multifunctional weak measurement system that can measure the refractive index and optical rotation of a solution," *Appl. Phys. Lett.*, vol. 114, no. 18, May 2019, Art. no. 181901, doi: 10.1063/1.5091468.
[21] L. Liu *et al.*, "A two-dimensional polarization interferometry based parallel scan angular surface plasmon resonance biosensor," *Rev. Sci. Instrum.*, vol. 82, no. 2, Feb. 2011, Art. no. 023109, doi: 10.1063/1.3553028.
[22] H. Shi *et al.*, "A symmetrical optical waveguide based surface plasmon resonance biosensing system," *Sensors Actuators B Chem.*, vol. 185, pp. 91–96, Aug. 2013, doi: 10.1016/j.snb.2013.05.005.
[23] W. Lu and W. M. Worek, "Two-wavelength interferometric technique for measuring the refractive index of salt-water solutions," *Appl. Opt.*, vol. 32, no. 21, pp. 3992–4002, Jul. 1993, doi: 10.1364/AO.32.003992.
[24] L. Luo *et al.*, "Precision improvement of surface plasmon resonance sensors based on weak-value amplification," *Opt. Express*, vol. 25, no. 18, pp. 21107–21114, Sep. 2017, doi: 10.1364/OE.25.021107.